

# Lamellar Diblock Copolymers on Rough Substrates: Self-Consistent Field Theory Studies

Xingkun Man,<sup>\*,†,‡</sup> Jiuzhou Tang,<sup>§</sup> Pan Zhou,<sup>⊥</sup> Dadong Yan,<sup>⊥</sup> and David Andelman<sup>\*,#,||</sup>

<sup>†</sup>Center of Soft Matter Physics and its Applications, and <sup>‡</sup>School of Physics and Nuclear Energy Engineering, Beihang University, Beijing 100191, China

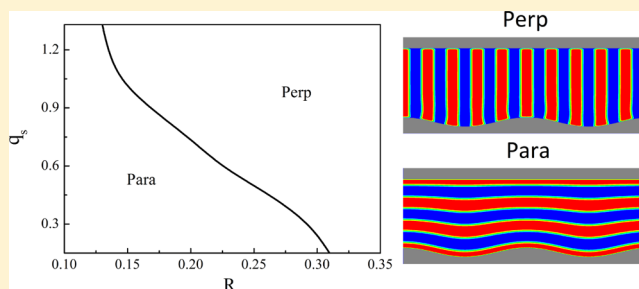
<sup>§</sup>Beijing National Laboratory Molecular Sciences (BNLMS), Laboratory of Polymer Physics and Chemistry, Institute of Chemistry, Chinese Academy of Sciences, Beijing 100190, China

<sup>||</sup>Kavli Institute for Theoretical Physics China, Chinese Academy of Sciences, Beijing 100190, China

<sup>⊥</sup>Department of Physics, Beijing Normal University, Beijing 100875, China

<sup>#</sup>Raymond and Beverly Sackler School of Physics and Astronomy, Tel Aviv University, Ramat Aviv 69978, Tel Aviv, Israel

**ABSTRACT:** We present numerical calculations of lamellar phases of diblock copolymers (BCP) confined between two surfaces, where the top surface is flat and the bottom one is corrugated. The corrugated substrate is assumed to have a single  $q$ -mode of lateral undulations with a wavenumber  $q_s$  and amplitude  $R$ . We focus on the effects of substrate roughness, parametrized by the dimensionless quantity,  $q_s R$ , on the relative stability between parallel and perpendicular orientations of the lamellar phase. The competition between film confinement, energy cost of elastic deformation, and gain in surface energy induces a parallel-to-perpendicular transition of the BCP lamellae. Employing self-consistent field theory (SCFT), we study the critical value,  $(q_s R)^*$ , corresponding to this transition. The  $(q_s R)^*$  value increases as a function of the surface preference toward one of the two BCP components and as a function of film thickness. But,  $(q_s R)^*$  decreases with increasing values of the Flory–Huggins parameter,  $N\chi_{AB}$ . Our findings are equivalent to stating that the critical  $(q_s R)^*$  value decreases as the BCP molecular weight or the natural BCP periodicity increases. We further show that the rough substrate can overcome the formation of parallel lamellae in cases where the top surface has a preference toward one of the two BCP components. Our results are in good agreement with previous experiments and highlight the physical conditions behind the perpendicular orientation of lamellar phases, as is desired in nanolithography and other industrial applications.



## I. INTRODUCTION

Block copolymers (BCP) are polymer systems where each of their chains is composed of two or more chemically distinct homopolymer blocks, covalently tethered together. As a result, BCP systems can spontaneously self-assemble at thermodynamical equilibrium into exquisitely ordered nanostructures.<sup>1</sup> The phase behavior of di-BCP melts, where each linear chain is composed of two blocks (denoted hereafter as A and B), has been studied extensively in recent decades and shows a rich variety of three-dimensional morphologies including lamellae, hexagonally close-packed cylinders, BCC packing of spheres, and gyroid networks.<sup>2,3</sup> The characteristic length scale in these well-defined structural phases ranges from a few nanometers to hundreds of nanometers and can offer an attractive alternative to patterning technology.<sup>4,5</sup> Besides applications in nanolithography, BCP films may offer novel opportunities in more traditional applications such as adhesive, hydrophobic, and antireflective surfaces as well as in the textile industry.<sup>6</sup>

Most of the BCP applications rely on casting them as thin films since this is the most appropriate form to construct a

surface pattern that can later be transferred onto a substrate, with potential applications as functional nanoscale devices.<sup>7</sup> A perpendicular orientation of BCP lamellae or cylinders, with respect to the underlying substrate, is usually desirable for most material and engineering applications.<sup>8</sup> During recent decades, various techniques have been developed to obtain such perpendicular lamellae or cylinders, including nonpreferential (neutral) interfaces,<sup>4,9</sup> topographically varying substrates<sup>10</sup> or top surfaces,<sup>11,12</sup> variations in polymeric block architecture,<sup>13,14</sup> and film thickness as well as solvent annealing.<sup>6</sup>

It is also possible to use corrugated substrates to obtain perpendicular BCP lamellae or cylinders. Sivaniah et al.<sup>15,16</sup> reported the effect of substrate roughness on the orientation of lamellae of symmetric poly(styrene)-*block*-poly(methyl methacrylate) (PS-*b*-PMMA). They identified a critical substrate roughness,  $(q_s R)^*$ , above which a perpendicular orientation was

**Received:** June 22, 2015

**Revised:** September 9, 2015

**Published:** October 6, 2015

observed, where  $q_s$  and  $R$  are the lateral wavenumber and its amplitude, respectively. They also found that the value of  $(q_s R)^*$  varies with BCP molecular weight (or the periodicity of BCP lamellae). In a more recent study, Kulkarni et al.<sup>17</sup> extended the results to include fractal substrate topography. A high fractal dimension of the rough substrate, in conjunction with an optimal surface energy of PS-*b*-PMMA in contact with the substrate, results in a complete perpendicular orientation of lamellar microdomains.

In a separate work, Kim et al.<sup>18</sup> investigated a film of PS-*b*-PMMA placed on an ordered nanoparticle (NP) monolayer. The substrate roughness is described by the parameter  $q_{\text{sub}} r$ , where  $q_{\text{sub}}$  and  $r$  are the wavenumber of substrate roughness and the radius of NP, respectively. A transition from parallel to perpendicular orientation of BCP lamellae or cylinders has been found by increasing the value of  $q_{\text{sub}} r$ . Furthermore, it was shown that the orientation of thin films of BCP is strongly influenced by the film thickness. This is due to the commensurability matching between film thickness and domain spacing.

In addition to the experimental situation, there are few theoretical works addressing the self-assembly of BCP films on corrugated surfaces. Turner and Joanny<sup>19</sup> and Tsori et al.<sup>20,21</sup> used the analogy between smectic liquid crystals and lamellar BCP and compared the phenomenological free energy of parallel and perpendicular lamellae on corrugated substrates. In refs 20 and 21 it was shown that for a fixed corrugation periodicity the perpendicular orientation is preferred for large corrugation amplitude and/or large lamellae periodicity. Moreover, for a fixed BCP natural periodicity, the perpendicular orientation is preferred for surfaces having large corrugation amplitude at short wavelengths.

Motivated by previous experimental works,<sup>17</sup> Ranjan et al.<sup>22</sup> conducted a scaling analysis of a single BCP lamella on fractal surfaces, which gives additional evidence that the substrate fractal dimension is an important factor in directing the orientation of BCP lamellae. Even more recently, Ye et al.<sup>23</sup> studied morphological properties of lamellae-forming di-BCPs on substrates with square-wave grating patterns by using self-consistent field theory (SCFT). They found three possible lamellar orientations with respect to the substrate and trench direction, but without addressing the key factors that determine the critical substrate roughness at the parallel-to-perpendicular phase transition of BCP microdomains.

We note that these previous studies have provided insight into how substrate roughness affects the relative stability of parallel and perpendicular BCP microdomains on nonflat surfaces. However, to date, systematic studies addressing the combined effect of substrate corrugation amplitude and lateral wavenumber, film thickness, and BCP periodicity on the domain orientation of BCP films are still missing. In this paper, we present a comprehensive and detailed SCFT study of di-BCP films constrained between a top flat surface and a bottom corrugated substrate. Our aim is to investigate the role played by substrate geometry, relative surface preference of the two BCP components, and BCP film properties, including film thickness, the Flory–Huggins parameter,  $N\chi_{AB}$ , between the two monomers, and the lamellar periodicity, on the parallel-to-perpendicular phase transition.

In the next section, we introduced the SCFT formalism and our numerical scheme. In section III, the corrugated surface and BCP film design are presented, while in section IV, we show the calculated phase diagrams of BCP lamellae on corrugated

substrates. Discussion of our results and comparison with previous models and experiments are presented in section V, followed by a summary and conclusions.

## II. THEORETICAL FRAMEWORK

**A. SCFT Scheme.** We use self-consistent field theory (SCFT) to investigate the lamellar phase of A/B di-BCP confined between two surfaces, where the top surface is flat and the bottom one is corrugated. We consider a melt of  $n_c$  chains, each composed of  $N = N_A + N_B$  monomers. For simplicity, the Kuhn length,  $b$ , is assumed to be the same for the A and B monomers, yielding an equality between the molar fraction and the volume one. The A-component molar fraction is  $f = N_A/N$ , and that of the B-component is  $1 - f$ . The BCP film has a total volume  $\Omega$ , lateral area  $\mathcal{A}$ , and thickness  $L = \Omega/\mathcal{A}$ . Hereafter, we concentrate on symmetric di-BCP, i.e.,  $f = 0.5$ .

In order to facilitate the numerical convergence, it is convenient to replace the sharp interface between the BCP film and the hard bounding surfaces by a “softer” wall with a smeared interface having a small width. This is done by introducing an artificial third (wall) component.<sup>1,24,25</sup> The local incompressibility condition is  $\phi_A(\mathbf{r}) + \phi_B(\mathbf{r}) + \phi_w(\mathbf{r}) = 1$ , where  $\phi_A$ ,  $\phi_B$ , and  $\phi_w$  are the A, B, and wall volume fractions within our simulation box, respectively. This condition is replaced with a compressible one, by adding an energetic penalty cost for local density deviations from the incompressibility condition. The penalty term is written as

$$\zeta(\phi_A(\mathbf{r}) + \phi_B(\mathbf{r}) + \phi_w(\mathbf{r}) - 1)^2 \quad (1)$$

and has a magnitude controlled by an “energy” parameter  $\zeta$  (in units of  $k_B T$ , where  $k_B$  is the Boltzmann constant and  $T$  is the temperature).

The direction parallel to the substrate is chosen to be along the  $x$ -direction, and the perpendicular one is in the  $y$ -direction. The system is assumed to be translational invariant in the third  $z$ -direction, which means that the numerical calculations are performed in a two-dimensional (2d) box. Hence,  $\Omega \rightarrow L_x \times L_y$  and  $\mathcal{A} \rightarrow L_x$ . All lengths, hereafter, are rescaled with the chain radius of gyration,  $R_g = (Nb^2/6)^{1/2}$ . With these conventions, the Hamiltonian of the BCP film confined between two surfaces can be expressed as a functional of two local fields<sup>1</sup>: a pressure field  $W_+(\mathbf{r})$  and an exchange potential field  $W_-(\mathbf{r})$

$$H[W_+, W_-] = C \int d^2\mathbf{r} \left( \frac{[W_-(\mathbf{r})]^2}{N\chi_{AB}} - \frac{2Nu}{N\chi_{AB}} \phi_w(\mathbf{r}) W_-(\mathbf{r}) + \frac{[W_+(\mathbf{r})]^2 - 2\zeta N \phi(\mathbf{r}) i W_+(\mathbf{r})}{N\chi_{AB} + 2N\zeta} \right) - C\Omega\bar{\phi} \ln Q[W_A, W_B] \quad (2)$$

where  $C = \rho_0 R_g^3 / N$  is a normalization factor,  $\rho_0 = (Nn_c + N_w) / \Omega$  is the total number density,  $\Omega$  is the entire volume (including the walls) of the simulation box,  $N_w$  is the total number of “wall monomers”, and  $\phi(\mathbf{r}) = \phi_A(\mathbf{r}) + \phi_B(\mathbf{r})$  is the dimensionless volume fraction of the polymer. The Flory–Huggins parameter between the A and B monomers is  $\chi_{AB}$ , and  $u = \chi_{wA} - \chi_{wB}$  is the relative interaction between the wall and the A/B components, where  $\chi_{wA}$  and  $\chi_{wB}$  are the interaction parameters between the wall (as a third component) and the A or B components, respectively. For example, a positive  $u > 0$  means that the surface prefers the A component. For simplicity, hereafter we absorb the factor of  $N$  into the definition of  $\zeta$  and  $u$ :  $N\zeta \rightarrow \zeta$  and  $Nu \rightarrow u$ .

The functional  $Q[W_A, W_B] = \Omega^{-1} \int d^2\mathbf{r} q(\mathbf{r}, s=1)$  is the single-chain partition function in the presence of the two conjugate fields,  $W_A(\mathbf{r}) = iW_+(\mathbf{r}) - W_-(\mathbf{r})$  and  $W_B(\mathbf{r}) = iW_+(\mathbf{r}) + W_-(\mathbf{r})$ , where the propagator  $q(\mathbf{r}, s)$  is the solution of the modified diffusion equation

$$\frac{\partial q(\mathbf{r}, s)}{\partial s} = \nabla^2 q(\mathbf{r}, s) - W(\mathbf{r}, s)q(\mathbf{r}, s) \quad (3)$$

satisfying the initial condition  $q(\mathbf{r}, s=0) = 1$ .  $W(\mathbf{r}) = W_A(\mathbf{r})$  for  $0 \leq s < f$  and  $W(\mathbf{r}) = W_B(\mathbf{r})$  for  $f \leq s \leq 1$ , where  $s$  is the curvilinear coordinate along the A/B chain contour. Finally,  $\bar{\phi} = \Omega^{-1} \int d^2\mathbf{r} \phi(\mathbf{r})$  is the polymer volume fraction averaged over  $\Omega$ .

Within the mean-field approximation, we can obtain the thermodynamic properties of the confined BCP film from a variational principle of the Hamiltonian in eq 2

$$\begin{aligned} \frac{\delta H[W_+, W_-]}{\delta(iW_+(\mathbf{r}))} &= 0 \\ \frac{\delta H[W_+, W_-]}{\delta W_-(\mathbf{r})} &= 0 \end{aligned} \quad (4)$$

This means that

$$\begin{aligned} \frac{\delta H}{\delta(iW_+(\mathbf{r}))} &= C \left[ \phi_A(\mathbf{r}) + \phi_B(\mathbf{r}) - \frac{2\zeta\phi(\mathbf{r}) + 2iW_+}{N\chi_{AB} + 2\zeta} \right] \\ \frac{\delta H}{\delta W_-(\mathbf{r})} &= C \left[ -\phi_A(\mathbf{r}) + \phi_B(\mathbf{r}) - \frac{2u\phi_w(\mathbf{r}) - 2W_-}{N\chi_{AB}} \right] \end{aligned} \quad (5)$$

Equation 4 can be solved numerically by solving the modified diffusion equation (eq 3) with spatially periodic boundary conditions and the following temporal relaxation equations:

$$\begin{aligned} \frac{\partial(iW_+(\mathbf{r}, t))}{\partial t} &= \frac{\delta H[W_+, W_-]}{\delta(iW_+)} \\ \frac{\partial W_-(\mathbf{r}, t)}{\partial t} &= -\frac{\delta H[W_+, W_-]}{\delta W_-} \end{aligned} \quad (6)$$

We use the well-documented pseudospectral method with FFTW to solve the modified diffusion equation and an explicit Euler scheme (first order in the iteration time) to update the field configurations to their saddle points. A detailed formulation of the numerical procedures for the SCFT model and their implementation to BCP systems can be found elsewhere.<sup>25–27</sup>

**B. Corrugated Substrate Design.** Our simulation setup is shown schematically in Figure 1, where the 2d simulation box of size  $L_x \times L_y$  includes the BCP film and the solid boundaries, and the average wall thickness is  $L_w$ . Hence, the average BCP film thickness  $L$  is given by  $L = L_y - 2L_w$ . The top surface is flat, while the bottom surface is corrugated, and is described by a height function

$$h(r_x) = R \cos(q_s r_x) \quad (7)$$

having a single  $q$ -mode with wavenumber  $q_s$  and amplitude  $R$ .

The wall density,  $\phi_w(\mathbf{r})$ , has a preassigned shape that is fixed (frozen) during the iterations. The top flat wall is modeled as a rectangle of size  $L_x \times L_w$  (Figure 1) and characterized by a smoothly varying wall function:

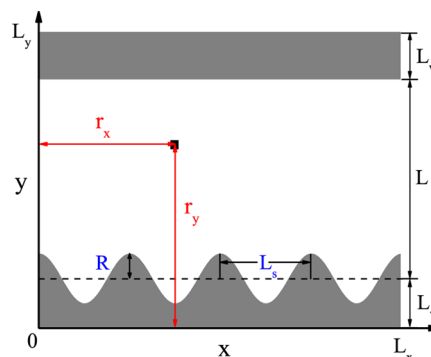


**Figure 1.** Schematic illustration of a BCP film confined between two surfaces. The two-dimensional calculation box has the size  $L_x \times L_y$ , where  $L = L_y - 2L_w$  is the averaged BCP film thickness, and  $L_w$  is the wall thickness (see text). The corrugated substrate is described by a height function:  $h(x) = R \cos(q_s r_x)$ , with lateral wavenumber  $q_s$  and amplitude  $R$ . Any point residing inside the film,  $\mathbf{r} = (r_x, r_y)$ , is parametrized by its  $x$ -axis and  $y$ -axis coordinates. The coordinate origin is taken at the bottom left corner of the simulation box. All lengths are rescaled by the chain radius of gyration,  $R_g$ .

$$\phi_w(\mathbf{r}) = \frac{1}{2} + \frac{1}{2} \tanh \left[ \frac{r_y - L_w - L}{\delta} \right] \quad (8)$$

where  $\delta$  parametrizes the interface width and  $r_y$  is the distance from the bottom box boundary. For the bottom corrugated surface, we impose a similar smoothly varying wall function

$$\phi_w(\mathbf{r}) = \frac{1}{2} - \frac{1}{2} \tanh \left[ \frac{r_y - R \cos(q_s r_x) - L_w}{\delta} \right] \quad (9)$$

where  $r_x$  is the distance to the left box boundary. Such a definition means that  $\phi_w(\mathbf{r}) = 1$  inside the wall region of the rectangular box and  $\phi_w(\mathbf{r}) = 0$  inside the BCP film. However, it generates a “soft” interface that is characterized by a narrow and smooth transition region of thickness  $\delta$ . Hereafter, we set  $\delta = 0.1$  and  $\zeta = 1000$  for all simulations, following previous simulation work.<sup>27</sup> Our results are not sensitive for values of  $\delta \leq 0.1$ , and consequently  $\delta = 0.1$  is chosen for convergence purposes. The value  $\zeta = 1000$  is large enough to model an incompressible system yet facilitate numerical converge.

### III. RESULTS

#### A. Parallel and Perpendicular Lamellar Orientations.

Symmetric BCPs yield thermodynamically stable lamellar phases with a bulk periodicity,  $L_0$ . The immediate effect of the corrugation can be seen in Figure 2. When the substrate roughness is large enough,  $q_s R \simeq 0.44$  (Figure 2a), the surface-induced distortion only propagates up to the second layer and all other lamellae are unperturbed. However, for small substrate roughness,  $q_s R \simeq 0.09$  as in Figure 2b, the lamellae follow the surface contour, and the distortions are longer range. It is important to note that the results are obtained for a finite film thickness where the top surface is flat and neutral ( $u_{\text{top}} = 0$ ). These results have smaller penetration length as compared with previous scaling<sup>19–21</sup> for infinite stacks of lamellae, where the penetration length scales as  $\sim q_0/q_s^2 \sim L_s^2/L_0$ .

Figure 3 shows examples of parallel and perpendicular lamellar phases in contact with a corrugated substrate in the strong segregation regime,  $N\chi_{AB} = 25$ . The bottom substrate in (a) and (b), having a moderate roughness,  $q_s R \simeq 0.25$ , is attractive to the A component (marked in red) with  $u = 3.05$ ,

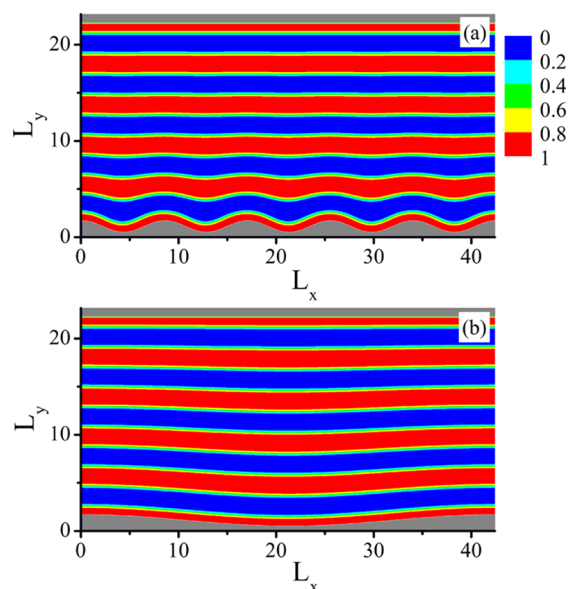


**Figure 2.** Parallel lamellar phase on a corrugated substrate. (a) The lateral wavelength  $q_s = 5(2\pi/L_x)$  and amplitude  $R = 0.6$ , resulting in a surface roughness,  $q_s R \approx 0.44$ . In this case, the surface-induced distortion penetrates only through the second layer. (b) A much smaller  $q_s R \approx 0.09$ , resulting from  $q_s = 2\pi/L_x$  and  $R = 0.6$ . Here the lamellar first four layers follow the surface topography. The color code corresponds to five discrete intervals of local monomer density  $0 \leq \phi_A(\mathbf{r}) \leq 1$ , as is depicted in (a). Other parameters are  $L_x = 42.5$ ,  $L = 21.25$ ,  $R = 0.6$ ,  $u = 3.3$ ,  $u_{\text{top}} = 0$ , and  $N\chi_{AB} = 25$ .

while the top surface is neutral ( $u_{\text{top}} = 0$ ). Clearly, the perpendicular lamellar phase ( $L_{\perp}$ ) in (a) is almost unperturbed, as compared to its bulk phase. However, the parallel one ( $L_{\parallel}$ ) in (b) adjusts its shape due to the surface corrugation. This is a result of the competition between the cost of BCP elastic deformation close to the corrugated surface and the gain in its

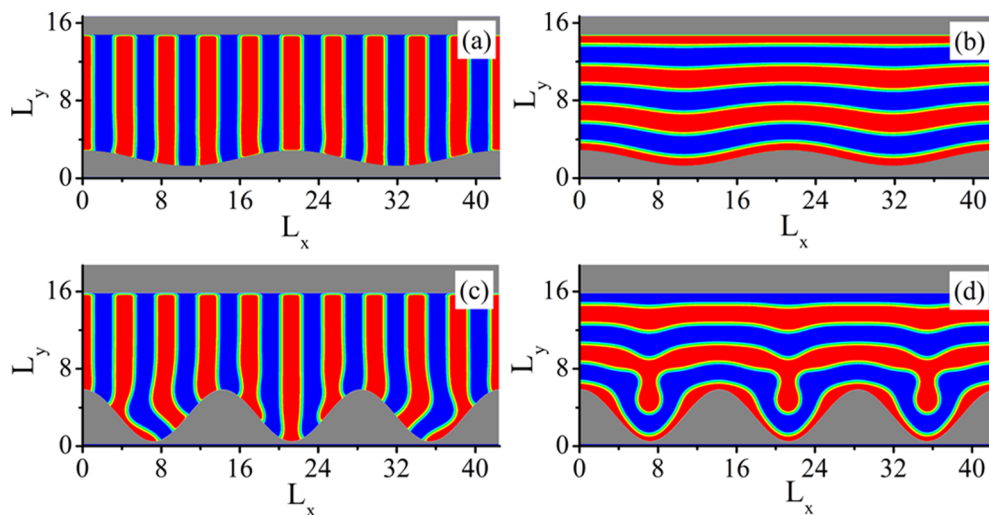
surface energy. The results both in (a) and (b) agree well with previous analytical results carried out by Tsori et al.<sup>20,21</sup>

For the case of large substrate roughness,  $q_s R \geq 1$ , the lamellae are strongly deformed, and it is hard to recognize whether their equilibrium structure is an  $L_{\perp}$  or  $L_{\parallel}$  phase. Such pronounced deformations are shown in Figure 3c,d, where the bottom substrate roughness is  $q_s R \approx 1.23$ , while all other conditions are the same as in (a) and (b). To be able to have meaningful predictions, we hereafter consider only substrates that have moderate roughness,  $q_s R < 1$ , and surface preference  $u$  that is less than the interaction between the A and B components,  $u < N\chi_{AB}$ .

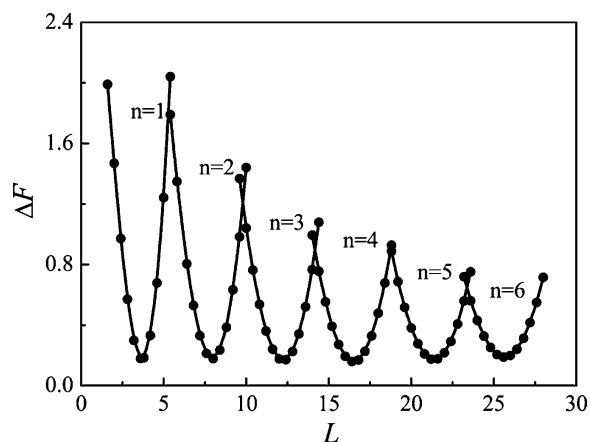
When the BCP film thickness,  $L$ , differs from an integer multiple of  $L_0$ , the BCP chains have to be stretched or compressed, as the total film volume is incompressible and space-filling (in our formalism,  $\zeta = 1000$  is large enough and models an incompressible system). In order to minimize such a confinement effect and focus mainly on how surface roughness affects the lamellar orientation, we adjust the box size such that the film thickness  $L$  corresponds to a local minimum of the  $L_{\parallel}$  free energy. This is done by investigating the free energy difference between parallel and perpendicular lamellae,  $\Delta F = F_{\parallel} - F_{\perp}$ , where  $F_{\parallel}$  and  $F_{\perp}$  are respectively the lamellar free energies of the two orientations.

Figure 4 shows the dependence of  $\Delta F$  on  $L$  with  $N\chi_{AB} = 25$ . We repeat the calculation of  $\Delta F$  for various lamellar layers,  $n = 1, 2, \dots, 6$ , between two flat and neutral surfaces. Clearly, the rescaled  $\Delta F$  has always a local minimum when  $L$  equals to an integer number times the natural periodicity,  $L = nL_0$ , in accord with previous SCFT calculations of Takahashi et al.<sup>27</sup> It is known that  $L_0$  depends on the value of  $N\chi_{AB}$ . Therefore, for different values of  $N\chi_{AB}$  we have to repeat this calculation and obtain the free energy in order to find the appropriate local minima, as in Figure 4.

It is important to note that when a thin BCP film is confined between two surfaces,  $L_0$  is also a function of the film thickness,  $L$ , and differs from its bulk value.<sup>27</sup> Moreover, the free energy of



**Figure 3.** SCFT calculation of BCP lamellae in contact with a moderate corrugated substrate in (a) and (b),  $q_s R \approx 0.25$ , and with a pronounced corrugated substrate in (c) and (d),  $q_s R \approx 1.23$ . For (a) and (b), the corrugation wavenumber is  $q_s = 2(2\pi/L_x)$  and its amplitude  $R = 0.85$ . The perpendicular lamellar phase ( $L_{\perp}$ ) in (a) is almost unperturbed compared to its bulk phase, while the parallel one ( $L_{\parallel}$ ) in (b) closely follows the surface contour. For (c) and (d),  $q_s = 3(2\pi/L_x)$  and  $R = 2.76$ . Both  $L_{\perp}$  in (c) and  $L_{\parallel}$  in (d) are strongly deformed. In all figure parts, calculations are done in the strong segregation limit,  $N\chi_{AB} = 25$ , resulting in a natural lamellar periodicity,  $L_0 = 4.25$ . The surface preference is  $u = 3.05$  for the bottom substrate and  $u_{\text{top}} = 0$  for the top surface. The color code are the same as those in Figure 2. The lateral box size is  $L_x = 42.5$ , and the average film thickness  $L = 12.75$ . All lengths are rescaled by  $R_g$  in all figures.



**Figure 4.** Free energy difference between parallel and perpendicular BCP lamellar orientations,  $\Delta F = F_{\parallel} - F_{\perp}$ , in units of  $n_c k_B T/L$ , as a function of the film thickness,  $L$ , where  $n_c$  is the number of chains and  $k_B T$  is the thermal energy. The parallel free energy,  $F_{\parallel}$ , is calculated separately for  $n = 1, 2, \dots, 6$  parallel lamellae confined between two flat neutral surfaces. The perpendicular free energy,  $F_{\perp}$ , corresponds to three periods of perfect perpendicular lamellae. The other parameters are  $L_x = 12.75$  and  $L_0 = 4.25$  (or, equivalently,  $N\chi_{AB} = 25$ ).

confined BCP films also depends on the surface preference field,  $u$ .<sup>24,28–30</sup> Therefore, the parameters  $N\chi_{AB}$ ,  $L$ , and  $u$  play an important role in determining whether the equilibrium orientation will be parallel ( $L_{\parallel}$ ) or perpendicular ( $L_{\perp}$ ), as will be further presented below.

We first compute the perp-to-para ( $L_{\perp}$ – $L_{\parallel}$ ) phase diagram (shown in Figure 5) in terms of the film rescaled thickness,

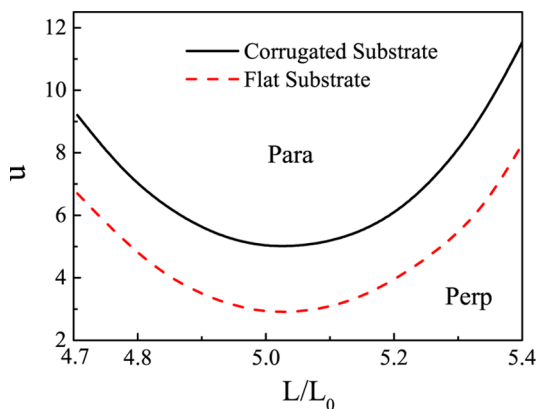


**Figure 5.**  $L_{\perp}$ – $L_{\parallel}$  phase diagram in terms of the rescaled film thickness  $L/L_0$  and substrate preference  $u$ , for a corrugated substrate (solid line), and for a flat substrate (dashed line). The top surface is flat and neutral ( $u_{\text{top}} = 0$ ). The lines separate between a stable  $L_{\perp}$  (perp) phase below and  $L_{\parallel}$  (para) phase above. The corrugated substrate is characterized by  $q_s = 9(2\pi/L_x) \approx 1.33$  and  $R = 0.45$ , yielding a roughness parameter,  $q_s R \approx 0.6$ . Other parameters are  $L_x = 42.5$  and  $L_0 = 4.25$  (or, equivalently,  $N\chi_{AB} = 25$ ).

$L/L_0$ , and bottom surface preference,  $u$ , for a corrugated substrate. For comparison, the calculation is then repeated for another system having a flat bottom surface, with the same parameters:  $L_x = 42.5$ ,  $u_{\text{top}} = 0$ , and  $N\chi_{AB} = 25$ . The film thickness varies around  $5L_0$ :  $4.7 \leq L/L_0 \leq 5.4$ . The wavenumber of the corrugated substrate is  $q_s = 9(2\pi/L_x)$ , while the corrugation magnitude is fixed,  $R = 0.45$ , resulting a substrate roughness  $q_s R \approx 0.60$ . The phase diagram is obtained

by starting with an initial condition of either an  $L_{\perp}$  phase of ten periods or an  $L_{\parallel}$  of five periods. After numerical convergence, the corresponding free energies are compared. The results show that the rough substrate greatly affects the phase diagram as compared with flat substrate. The  $L_{\perp}$ – $L_{\parallel}$  phase-transition line for the corrugated case is shifted upward, which means that the  $L_{\perp}$  phase has a larger stability range for rough substrates than for flat ones. This conclusion qualitatively agrees with previous analytical and experimental studies.<sup>16,18,21</sup> It shows that rough substrates, just like chemical-patterned substrates and nano-imprint surfaces,<sup>29</sup> can enhance the stability of the  $L_{\perp}$  phase as compared with a flat substrate with the same surface preference field,  $u$ .

**B. Substrate Effect on Para-to-Perp Transition.** We proceed by studying quantitatively the effect of substrate roughness on the relative stability of the  $L_{\perp}$  and  $L_{\parallel}$  phases. We focus on the role played by (i) the substrate geometry, including lateral wavenumber,  $q_s = 2\pi/L_s$ , and roughness amplitude,  $R$ , (ii) the relative surface preference toward the two BCP components,  $u$ , and (iii) BCP film properties, including film thickness,  $L$ , the Flory–Huggins parameter,  $N\chi_{AB}$ , and the BCP natural periodicity, on the  $L_{\parallel}$ – $L_{\perp}$  phase transition.

Figure 6 shows the  $L_{\parallel}$ – $L_{\perp}$  phase diagram in terms of the corrugation parameters,  $R$  and  $q_s$ , for a fixed bottom substrate

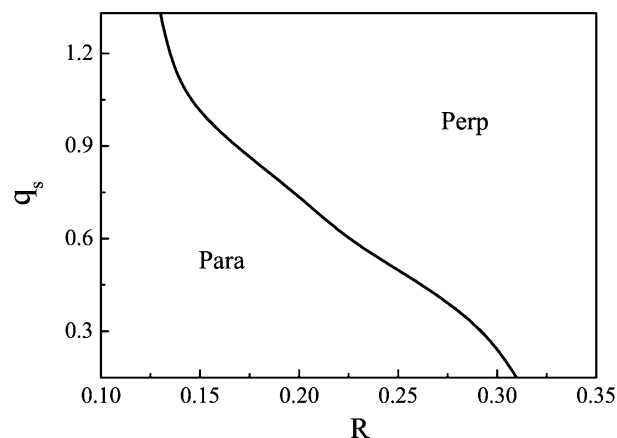


**Figure 6.**  $L_{\perp}$ – $L_{\parallel}$  phase diagram in terms of  $R$  and  $q_s$ . The parameters used are  $L = 21.25$ ,  $L_x = 2L = 42.5$ ,  $L_0 = 4.25$  (or, equivalently,  $N\chi_{AB} = 25$ ),  $u = 3.05$ , and  $u_{\text{top}} = 0$ .

preference ( $u = 3.05$ ) and a flat neutral top surface ( $u_{\text{top}} = 0$ ). For fixed  $q_s$ , while increasing  $R$ , an  $L_{\parallel}$ -to- $L_{\perp}$  phase transition is reached because the elastic deformation of the  $L_{\parallel}$  lamellae along the corrugated surface becomes bigger, favoring the  $L_{\perp}$  orientation. For fixed value of  $R$ , an increase of  $q_s$  also induces an  $L_{\parallel}$ -to- $L_{\perp}$  phase-transition. This can be understood as smaller  $q_s$  (while keeping  $R$  constant) means that the substrate effectively is flatter, and the  $L_{\parallel}$  lamellae are losing less elastic deformation energy. In the limit of  $q_s \rightarrow 0$  (corresponding to an unrealizable large simulation box), the substrate approaches to a flat substrate. Then, the  $L_{\parallel}$  phase will be more stable than  $L_{\perp}$  because of the substrate preference toward one of the two BCP components.

As discussed in section III.A, the surface preference,  $u$ , is an important factor in determining the final lamellar orientation. Moreover,  $q_s R$  is usually used to parametrize the substrate roughness in experiments. We investigate the effects of the substrate  $u$  on the critical value,  $(q_s R)^*$ , corresponding to the  $L_{\parallel}$ – $L_{\perp}$  phase transition, while keeping the top surface neutral

( $u_{\text{top}} = 0$ ) and flat (see Figure 7). Our results show that  $(q_s R)^*$  increases as a function of  $u$ . This means that for larger  $u$ , larger

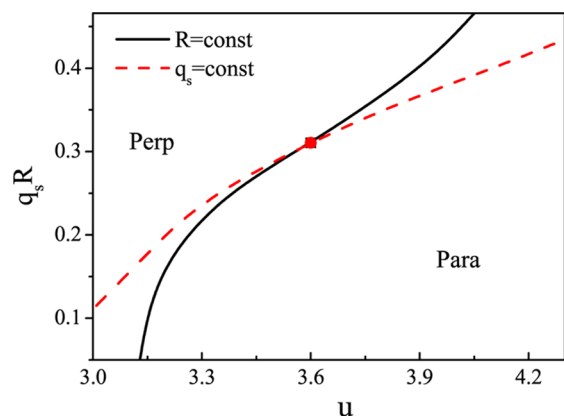


**Figure 7.** Comparison between two ways (solid and dashed lines) to obtain the  $L_{\parallel}$ -to- $L_{\perp}$  phase-transition plotted in the  $(q_s R, u)$  plane. The solid line is calculated for constant  $R = 0.35$ . The roughness wavenumber  $q_s = n_s(2\pi/L_x)$  is varied discretely, where  $n_s = 1, 2, 3, \dots, 9$  is the number of periods within the lateral box width. The dashed line corresponds to constant  $q_s = 6(2\pi/L_x)$ , while  $R$  varies from 0.1 to 0.5. The results show that  $(q_s R)^*$  at the phase transition increases faster by varying  $q_s$  than by varying  $R$ . All other parameters are the same as in Figure 6.

substrate roughness is needed to induce an  $L_{\parallel}$ -to- $L_{\perp}$  phase transition. This is due to the competition between the energy cost of elastic deformation and gain in surface energy. Increasing  $q_s R$  leads to more elastic deformation in the  $L_{\parallel}$  phase as compared with  $L_{\perp}$ , resulting in a phase transition from an  $L_{\parallel}$  to an  $L_{\perp}$  phase. Oppositely, increasing  $u$  makes the  $L_{\parallel}$  phase more stable because of the gain in surface energy, leading to a phase transition from  $L_{\perp}$  to  $L_{\parallel}$ .

We present in Figure 7 two ways to change the values of  $q_s R$ . First, we fix the corrugation amplitude,  $R = 0.35$ , and change the wavenumber discretely by taking these values as  $q_s = n_s(2\pi/L_x)$ , where  $n_s = 1, 2, \dots, 9$  is the number of lateral periods of the substrate. Next, we fix  $q_s = 6(2\pi/L_x)$  and change  $R$  from 0.1 to 0.5. The simulation box size is set to  $L_x = 42.5$ ,  $L = 21.25$ , and  $N\chi_{AB} = 25$ . For the calculations,  $L_{\perp}$  has ten BCP lamellar periods as its initial condition while  $L_{\parallel}$  has five. After convergence, the  $L_{\perp}$  and  $L_{\parallel}$  free energies are compared, and clearly, for both phases,  $(q_s R)^*$  is an increasing function of  $u$ . However, for the same value of  $u$ , the value of  $(q_s R)^*$  is different for constant  $R$  and constant  $q_s$ , with a  $(q_s R)^*$  difference of the order of  $10^{-2}$ . This indicates that  $q_s R$  is not exactly a scaling field for the  $L_{\parallel}$ - $L_{\perp}$  phase-transition. The reason is that the contour length of the substrate has a small difference (also on the order of  $10^{-2}$ ) for different combinations of  $q_s$  and  $R$ , while keeping their product  $q_s R$  the same. Such differences will further result in a different elastic deformation and surface energies of the film.

### C. Film Effect on the Para-to-Perp Phase Transition.

Another important parameter that affects  $(q_s R)^*$  is the BCP film thickness,  $L$ . Table 1 presents the dependence of  $(q_s R)^*$  on

**Table 1.** Critical Substrate Roughness for Various Rescaled BCP Film Thicknesses

$L/L_0$	2	3	4	5	6
$(q_s R)^*$	0.15	0.17	0.18	0.21	0.26

$L$ , obtained with fixed preference of the bottom and top surfaces,  $u = 3.05$  and  $u_{\text{top}} = 0.15$ , respectively. We add a small top surface preference,  $u_{\text{top}} > 0$ , to mimic the experiments, where BCPs usually have nonzero preference in their surface interaction with the air. More discussion about the top surface preference effects on the  $L_{\parallel}$ - $L_{\perp}$  phase transition will be addressed in section IV. As mentioned in Figure 4, we choose the film thickness  $L$  to be an integer multiple of the  $L_{\parallel}$  periodicity, i.e.,  $L = nL_0$ , where  $n = 2, 3, \dots, 6$ , in order to minimize the film confinement effects. The  $L_{\parallel}$  free energy is compared with the  $L_{\perp}$  one with  $L_x = 2L_0$ , while all other parameters are kept the same. The numerical results indicate that  $(q_s R)^*$  increases for thicker BCP film. This is understandable because the elastic deformation induced by the corrugated substrate is a surface effect with limited penetration into the BCP film. Therefore, larger  $q_s R$  values are needed to induce the  $L_{\parallel}$ -to- $L_{\perp}$  phase transition for thicker films.

Finally, we examine the effect of  $N\chi_{AB}$  (or  $L_0$ ) on the  $L_{\parallel}$ - $L_{\perp}$  phase transition in Figure 8. As mentioned above, varying  $N\chi_{AB}$  will also change the BCP lamellar periodicity,  $L_0$ . In order to stay in the minimal confinement free energy, we set  $L = nL_0$ , where  $L_0$  varies for different  $N\chi_{AB}$ . Because the minimum in  $F_{\perp}$  corresponds to  $L_x = nL_0$ , we obtain the value of  $L_0$  for different  $N\chi_{AB}$  by examining the dependence of  $F_{\perp}$  on  $L_x$ , while keeping  $L$  fixed. After determining the values of  $L_0$ , we can adjust our simulation box accordingly. The  $L_0$  values for different  $N\chi_{AB}$  are shown in Table 2, where it can be seen that  $L_0$  is an increasing function of  $N\chi_{AB}$ .<sup>36</sup> For all calculations in Figure 8, the parameters are  $L_x = 2L_0$ ,  $u = 3.05$ , and  $u_{\text{top}} = 0.15$ . The  $L$  values for different  $N\chi_{AB}$  are set to fulfill  $L = 3L_0$  (see Table 2).

From Figure 8a, one sees that  $(q_s R)^*$  decreases as  $N\chi_{AB}$  increases. This can be understood because when  $N\chi_{AB}$  increases, the lamellar periodicity,  $L_0$ , also increases, and the local deformation of BCP lamellae becomes larger. For example, in the limit of  $q_s/q_0 \rightarrow 0$ , the corrugated substrate is equivalent to a flat one, and the BCP lamellae will not be deformed anymore, resulting in no elastic deformation. In other words, the energy cost of the elastic deformation increases as  $q_s/q_0$  increases. Then, smaller values of  $(q_s R)^*$  are needed to induce the  $L_{\parallel}$ -to- $L_{\perp}$  phase transition. The tendency of  $(q_s R)^*$  to decrease when  $L_0$  increases is shown in Figure 8b and is consistent with the results in Table 1. When  $L_0$  increases, it means that the value of  $L/L_0$  in Table 1 decreases, and the same tendency of  $(q_s R)^*$  on  $L_0$  is obtained.

## IV. DISCUSSION

**A. Comparison with Experiments.** Our study has been motivated by the experimental works of Sivaniyah et al.<sup>16</sup> and Char's group.<sup>18</sup> In ref 16, PS-*b*-PMMA films are casted onto an array of polyimide (PIM) substrates having different roughness. The study found the critical roughness of the PIM substrate,  $(q_s R)^*$ , separating the stable  $L_{\perp}$  lamellae for  $q_s R > (q_s R)^*$  from the region where the  $L_{\parallel}$  lamellae are more stable,  $q_s R < (q_s R)^*$ . In a more recent work by Char's group,<sup>18</sup> both lamellar and cylindrical phases of PS-*b*-PMMA were spin-coated onto two different substrates covered with an ordered nanoparticle (NP) monolayer. In the first setup, the NP size is  $R = 6$  nm and its repeat period is  $q_s \approx 0.75$  nm<sup>-1</sup>, resulting in  $q_s R \approx 4.5$ . For the second setup, the NP size is  $R = 22$  nm and the repeat period is  $q_s \approx 0.26$  nm<sup>-1</sup>, which leads to  $q_s R \approx 5.72$ . For both lamellae and cylinders,  $L_{\parallel}$  orientation was obtained in the first case ( $q_s R \approx 4.5$ ), and  $L_{\perp}$  orientation was obtained for the second one ( $q_s R \approx 5.72$ ). The conclusion from these experiments is

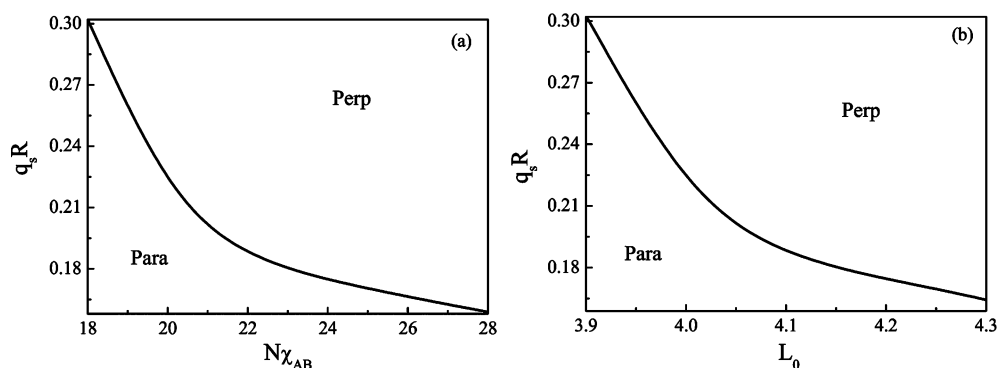


**Figure 8.** (a)  $L_{\perp}$ – $L_{\parallel}$  phase diagram in terms of  $q_s R$  and the interaction between A and B blocks,  $N\chi_{AB}$ . The box size is adjusted to have two periods of  $L_{\perp}$  and three periods of  $L_{\parallel}$  for various values of  $N\chi_{AB}$ . (b) Equivalent  $L_{\perp}$ – $L_{\parallel}$  phase diagram expressed in terms of  $L_0$  and  $q_s R$ . Other parameters are  $u = 3.05$ ,  $u_{\text{top}} = 0.15$ , and  $q_s = 2\pi/L_x$ .

**Table 2. Lamellar Periodicity,  $L_0$ , and Average Film Thickness,  $L = 3L_0$ , for Various  $N\chi_{AB}$  Values**

$N\chi_{AB}$	18	20	22	25	28
$L_0$	3.90	4.00	4.10	4.25	4.35
$L$	11.7	12.00	12.30	12.75	13.05

that increasing the substrate roughness can induce an  $L_{\parallel}$ -to- $L_{\perp}$  phase transition. All of our results nicely support these findings, although we can justify less our SCFT results in a quantitative manner for  $q_s R > 1$ .

Sivaniah et al.<sup>16</sup> have also shown that the value of  $(q_s R)^*$  varies with the BCP molecular weight. Keeping all experimental conditions the same, the value of  $(q_s R)^*$  for 38K-38K PS-*b*-PMMA was found to be  $0.37 \pm 0.02$ , and for 18K-18K it is  $0.41 \pm 0.02$ . Furthermore, the natural periodicity for the 38K-38K system is  $L_0 = 36.7$  nm, and for 18K-18K it is  $L_0 = 28.6$  nm. Because the experiments were conducted for only two BCP chain lengths, it was not possible to infer any trend of lower  $(q_s R)^*$  values for higher molecular weights. However, our results indicate such a trend, where the values of  $L_0$  increase from 3.90 to 4.35, and corresponds to a decrease of  $(q_s R)^*$ .

**B. Comparison with Previous Models.** In a closely related analytical study, Tsori et al.<sup>20,21</sup> used the analogy between smectic liquid crystals and lamellar BCP, compared the phenomenological free energies of  $L_{\parallel}$  and  $L_{\perp}$  phases on corrugated substrate, and studied their relative stability. Their results can be summarized by the following three findings. While keeping all other parameters fixed, these authors found that (i) increasing  $R$  induces an  $L_{\parallel}$ -to- $L_{\perp}$  phase transition, (ii) increasing  $q_s$  results in an  $L_{\perp}$ -to- $L_{\parallel}$  phase-transition, and (iii) increasing  $q_0$  leads to an  $L_{\parallel}$ -to- $L_{\perp}$  phase transition. Our findings agree with the first finding of Tsori et al. as well as with the experimental findings discussed in section IV.A. Increasing the value of  $R$  (while all other parameters are fixed) means larger substrate roughness, and therefore it induces an  $L_{\parallel}$ – $L_{\perp}$  phase transition. However, the second and third findings of Tsori et al. are contrary to experimental trends<sup>16</sup> as well as to our SCFT calculations.

One of the results of Tsori et al.<sup>20,21</sup> is that  $F_{\parallel}$  is an increasing function of the lateral wavelength,  $F_{\parallel} \sim (R/q_s)^2 \sim q_s^{-2}$ , while  $F_{\perp}$  scales as  $(q_s R)^2$ . However, our SCFT results show an opposite trend for  $F_{\parallel} \sim (q_s R)^2 \sim q_s^2$ , while the same scaling for  $F_{\perp} \sim (q_s R)^2$ . This behavior of the two free energies is shown in Figure 9, and in the inset the scaling with  $(q_s R)^2$  can be clearly seen. We note that in an even earlier work by Turner and

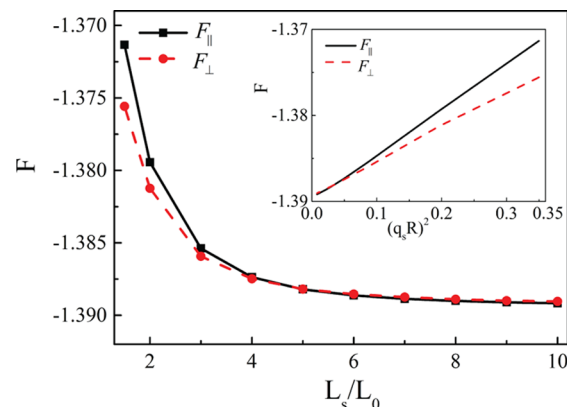


**Figure 9.** Dependence of  $F_{\parallel}$  and  $F_{\perp}$  on the lateral wavelength,  $L_s = 2\pi/q_s$ . The value of  $L_s$  varies from  $1.5L_0$  to  $10L_0$  with  $L_0 = 4.25$ . In the inset, the two free energies are shown to scale, within a good approximation, with  $(q_s R)^2$ . Other parameters are  $L_x = 42.5$ ,  $L = 21.25$ ,  $R = 0.6$ ,  $u = 3.3$ ,  $u_{\text{top}} = 0$ , and  $N\chi_{AB} = 25$ .

Joanny<sup>19</sup> the free energies of both  $F_{\parallel}$  and  $F_{\perp}$  stack on a corrugated substrate were found to scale as  $(q_s R)^2$  (while all other parameters are fixed). We conjecture that the discrepancy between our SCFT and the previous analytical results<sup>19–21</sup> is due mainly to two reasons. One is the fact that our stack has a finite width and the top surface is affecting the penetration length and hence the delicate balance between the two orientations. The second reason is related to local deformations of BCP chains close to the corrugated substrate. These deformations are not well described within models that draw on the analogy with a continuum theory of smectic liquid crystals, and which assumes small and gradual deformations.

**C. Non-Neutral Air/Polymer Interface.** It is known that when the top surface (polymer film/air) has a preference toward one of the two BCP blocks, it can induce an  $L_{\parallel}$  orientation inside the film. In many applications (e.g., in nanolithography), it is highly desired to circumvent the  $L_{\parallel}$  phase by using the so-called “top coats”.<sup>33–35</sup> Moreover, Khanna et al.<sup>13</sup> in experiments and Matsen<sup>14</sup> in theory have shown that the BCP architecture can also affect the polymer/air surface tension and facilitates the formation of  $L_{\perp}$  lamellae.

Figure 10 shows a comparison of the  $L_{\parallel}$ – $L_{\perp}$  phase diagram in terms of  $R$  and  $q_s$  between a system with a top surface field,  $u_{\text{top}} = 0.15$ , and a second system with a neutral top surface,  $u_{\text{top}} = 0$  (same as in Figure 5). From Figure 10 it can be seen to what degree the nonzero top surface affects the relatively

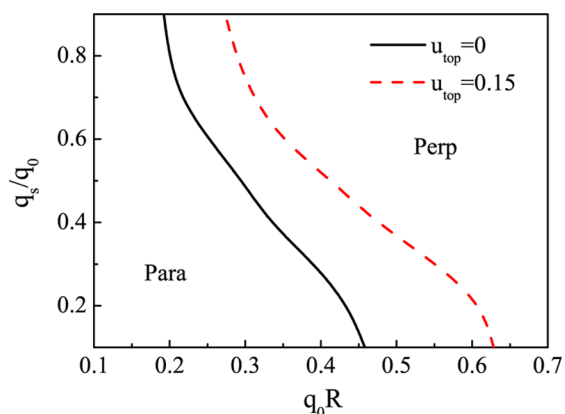


**Figure 10.** Comparison of the  $L_{\perp}$ – $L_{\parallel}$  phase diagram in the  $(q_0 R, q_s/q_0)$  plane, between a neutral top surface  $u_{\text{top}} = 0$  (solid black line) and a non-neutral one,  $u_{\text{top}} = 0.15$  (dashed red line). All other parameter values are as in Figure 6.

stability of the  $L_{\perp}$  and  $L_{\parallel}$  phases. When a small surface preference is added to the top surface, the  $L_{\parallel}$ – $L_{\perp}$  phase-transition line shifts to the right (the red dashed line); namely, the transition value  $(q_s R)^*$  increases. Our study is instrumental as it shows a possible solution utilizing a rough substrate to overcome the parallel orientation induced by the commonly found air/film preference,  $u_{\text{top}} \neq 0$ . Therefore, combining the “top coats”, varying BCP architecture, as well as employing rough substrates may offer an effective way to obtain perpendicular orientation of BCP nanostructures, even in cases where BCPs have significant different surface tension between the air and the two blocks of the BCP.

## V. CONCLUSIONS

In this article, we address the influence of a nonflat substrate on the relative stability between the two orientations,  $L_{\parallel}$  and  $L_{\perp}$ , of lamellar BCP phases. The thin lamellar film is confined between a top flat surface and bottom corrugated substrate of a shape,  $R \cos(q_s x)$ , with a single  $q$ -mode of lateral undulations. The competition between the energy cost of elastic deformation and gain in surface energy of BCP lamellae results in an  $L_{\parallel}$ – $L_{\perp}$  phase transition.

We comprehensively and systematically studied the combined effect of the rough substrate with lateral wave-number,  $q_s$ , and magnitude  $R$ , as well as the interface energy between the BCP and the surface, film thickness, and the Flory parameter on the  $L_{\parallel}$ -to- $L_{\perp}$  phase transition. Our results show that increasing the substrate roughness,  $q_s R$ , induces an  $L_{\parallel}$ -to- $L_{\perp}$  phase transition. Moreover, the critical value of the substrate roughness,  $(q_s R)^*$ , corresponding to the  $L_{\parallel}$ – $L_{\perp}$  phase transition, increases as the surface preference toward one of the two blocks,  $u$ , increases, or as the film thickness becomes thicker. On the other hand, it decreases when the Flory parameter,  $N\chi_{AB}$ , or the natural periodicity,  $L_0$ , increases.

We focused in this study on a few key factors that enhance or induce the phase transition from  $L_{\parallel}$  into the  $L_{\perp}$  phase, as is desired in applications. As detailed in the section IV, our predictions are consistent with several experimental findings. Furthermore, as our study is systematic, its predictions can be further tested experimentally by using di-BCP with different chain lengths and periodicities, and by changing in a tunable fashion the corrugated substrate, the top surface preference as

well as the film thickness, in order to determine the optimal condition for the enhance stability of the  $L_{\perp}$  phase.

In addition to the effect of substrate roughness on the parallel-to-perpendicular orientation transition, corrugated substrates have been shown to improve in-plane ordering of thin BCP films.<sup>10,31,32</sup> We hope that in the future more detailed 3d calculations will shed more light on various possibilities that nonflat substrates may improve the in-plane ordering and defect annihilation of BCP lamellar phases.

## ■ AUTHOR INFORMATION

### Corresponding Authors

\*E-mail [manxk@buaa.edu.cn](mailto:manxk@buaa.edu.cn) (X.M.).

\*E-mail [andelman@post.tau.ac.il](mailto:andelman@post.tau.ac.il) (D.A.).

### Author Contributions

X.M. and J.T. have equal contributions to this work.

### Notes

The authors declare no competing financial interest.

## ■ ACKNOWLEDGMENTS

This work was supported in part by grants 21404003, 21434001, and 21374011 of the National Natural Science Foundation of China (NSFC), the 973 program of the Ministry of Science and Technology (MOST) 2011CB808502, and the Fundamental Research Funds for the Central Universities. We thank Henri Orland and Yoav Tsori for useful discussions and comments. D.A. acknowledges support from the Israel Science Foundation (ISF) under Grant No. 438/12 and the United States–Israel Binational Science Foundation (BSF) under Grant No. 2012/060.

## ■ REFERENCES

- (1) Fredrickson, G. H. *The Equilibrium Theory of Inhomogeneous Polymers*; Oxford University Press: New York, 2006.
- (2) Matsen, M. W.; Schick, M. *Phys. Rev. Lett.* **1994**, *72*, 2660.
- (3) Bates, F. S.; Schulz, M. F.; Khandpur, A. K.; Förster, S.; Rosedale, J. H.; Almdal, K.; Mortensen, K. *Faraday Discuss.* **1994**, *98*, 7.
- (4) Kim, H.-C.; Park, S.-M.; Hinsberg, W. D. *Chem. Rev.* **2010**, *110*, 146.
- (5) Bates, F. S.; Fredrickson, G. H. *Annu. Rev. Phys. Chem.* **1990**, *41*, 525.
- (6) Sinturel, C.; Vayer, M.; Morris, V. M.; Hillmyer, M. A. *Macromolecules* **2013**, *46*, 5399.
- (7) Hamley, I. W. *Prog. Polym. Sci.* **2009**, *34*, 1161.
- (8) Bates, C. M.; Maher, M. J.; Janes, D. W.; Ellison, C. J.; Willson, C. G. *Macromolecules* **2014**, *47*, 2.
- (9) Liu, P.-H.; Thébaud, P.; Guenoun, P.; Daillant, J. *Macromolecules* **2009**, *42*, 9609.
- (10) Park, S.-M.; Berry, B. C.; Dobisz, E.; Kim, H.-C. *Soft Matter* **2009**, *5*, 957.
- (11) Man, X.-K.; Andelman, D.; Orland, H.; Thébaud, P.; Liu, P.-H.; Guenoun, P.; Daillant, J.; Landis, S. *Macromolecules* **2011**, *44*, 2206.
- (12) Thébaud, P.; Niedermayer, S.; Landis, S.; Chaix, N.; Guenoun, P.; Daillant, J.; Man, X.-K.; Andelman, D.; Orland, H. *Adv. Mater.* **2012**, *24*, 1952.
- (13) Khanna, V.; Cochran, E. W.; Hexemer, A.; Stein, G. E.; Fredrickson, G. H.; Kramer, E. J.; Li, X.; Wang, J.; Hahn, S. F. *Macromolecules* **2006**, *39*, 9346.
- (14) Matsen, M. W. *Macromolecules* **2010**, *43*, 1671.
- (15) Sivaniah, E.; Hayashi, H.; Iino, M.; Hashimoto, T.; Fukunaga, K. *Macromolecules* **2003**, *36*, 5894.
- (16) Sivaniah, E.; Hayashi, H.; Matsubara, S.; Kiyono, S.; Hashimoto, T.; Fukunaga, K.; Kramer, E. J.; Mates, T. *Macromolecules* **2005**, *38*, 1837.

- (17) Kulkarni, M. M.; Yager, K. G.; Sharma, A.; Karim, A. *Macromolecules* **2012**, *45*, 4303.
- (18) Kim, T.; Wooh, S.; Son, J. G.; Char, K. *Macromolecules* **2013**, *46*, 8144.
- (19) Turner, M. S.; Joanny, J.-F. *Macromolecules* **1992**, *25*, 6681.
- (20) Tsori, Y.; Andelman, D. *Macromolecules* **2003**, *36*, 8560.
- (21) Tsori, Y.; Sivaniah, E.; Andelman, D.; Hashimoto, T. *Macromolecules* **2005**, *38*, 7193.
- (22) Ranjan, A.; Kulkarni, M.; Karim, A.; Sharma, A. *J. Chem. Phys.* **2012**, *136*, 094903.
- (23) Ye, X.; Edwards, B. J.; Khomami, B. *Macromol. Rapid Commun.* **2014**, *35*, 702.
- (24) Matsen, M. W. *J. Chem. Phys.* **1997**, *106*, 7781.
- (25) Bosse, A. W.; García-Cervera, C. J.; Fredrickson, G. H. *Macromolecules* **2007**, *40*, 9570.
- (26) Hur, S.-M.; García-Cervera, C. J.; Kramer, E. J.; Fredrickson, G. H. *Macromolecules* **2009**, *42*, 5861.
- (27) Takahashi, H.; Laachi, N.; Delaney, K. T.; Hur, S.-M.; Weinheimer, C. J.; Shykind, D.; Fredrickson, G. H. *Macromolecules* **2012**, *45*, 6253.
- (28) Geisinger, T.; Müeller, M.; Binder, K. *J. Chem. Phys.* **1999**, *111*, 5241.
- (29) Man, X.-K.; Andelman, D.; Orland, H. *Macromolecules* **2010**, *43*, 7261.
- (30) Tsori, Y.; Andelman, D. *Eur. Phys. J. E: Soft Matter Biol. Phys.* **2001**, *5*, 605.
- (31) Park, S.; Lee, D. H.; Xu, J.; Kim, B.; Hong, S. W.; Jeong, U.; Xu, T.; Russell, T. P. *Science* **2009**, *323*, 1030.
- (32) Vega, D. A.; Gómez, L. R.; Pezzutti, A. D.; Pardo, F.; Chaikin, P. M.; Register, R. A. *Soft Matter* **2013**, *9*, 9385.
- (33) Bates, C. M.; Seshimo, T.; Maher, M. J.; Durand, W. J.; Cushen, J. D.; Dean, L. M.; Blachut, G. J.; Willson, C. G. *Science* **2012**, *338*, 775.
- (34) Yoshida, H.; Suh, H. S.; Ramirez-Herunandez, A.; Lee, J. I.; Aida, K.; Wan, L.; Ishida, Y.; Tada, Y.; Ruiz, R.; de Pablo, J.; Nealey, P. F. *J. Photopolym. Sci. Technol.* **2013**, *26*, 55.
- (35) Kim, E.; Kim, W.; Lee, K. H.; Ross, A. C.; Son, J. G. *Adv. Funct. Mater.* **2014**, *24*, 6981.
- (36) Sivaniah, E.; Matsubara, S.; Zhao, Y.; Hashimoto, T.; Fukunaga, K.; Kramer, E. J.; Mates, T. E. *Macromolecules* **2008**, *41*, 2584.